Inkjet Printing at Megahertz Frequency

John C. Miers, Wenchao Zhou
The AM³ Lab, Department of Mechanical Engineering, University of Arkansas at Fayetteville
Fayetteville, AR, United States of America; email: jcmiers@uark.edu zhouw@uark.edu

Inkjet printing enables more efficient, economic, scalable manufacturing for a wider variety of materials, than other traditional additive techniques. However, the jetting frequency of commercial droplet-on-demand inkjet techniques is mostly limited to ~10 kHz. This paper presents an investigation of the possibility of jetting at megahertz frequencies in order to boost the productivity of inkjet by ~100 times. The key to this problem is rooted in droplet formation dynamics, a subject that has been extensively studied for over 300 years. Hence, the focus of this paper is to understand the limitations of generating droplets at a megahertz frequency and explore possible solutions for overcoming these limitations. The paper begins with a review of literature on the dynamics of droplet formation. A numerical model is then developed for the simulation of droplet formation dynamics. The numerical model is validated against available experimental data from the literature. Aided by insights gained from scaling analysis, the validated model is then used to study the effects of different process parameters on high frequency jetting. The study finds energy density input to the nozzle is the key to achieve megahertz frequency printing.

1. INTRODUCTION

Inkjet printing, as an elegant digital material distribution technique, has become an increasingly popular additive manufacturing technique for various applications, such as printed electronics, fabrication of OLED displays, and solar cells [1] [2] [3] [4] [5] [6] [7]. At the core of inkjet printing, is droplet generation, which is a common module for all different applications of inkjet and determines the productivity and quality of the prints. Historically two conceptually different approaches have been developed: continuous inkjet and drop-on-demand (DOD) inkjet [8]. In a continuous inkjet system, high pressure is applied to a fluid reservoir to produce a continuous fluid stream of approximately the diameter of the nozzle, which breaks into droplets after leaving the nozzle due to Plateau-Rayleigh instability [9]. In contrast, a DOD inkjet creates a short-duration jet that condenses into a single droplet of the desired diameter. Due to its simplicity and precise control of droplets, DOD has become the mainstream inkjet technique [10]. Many different approaches have been explored for DOD inkjets, including electrohydrodynamic jetting, thermal jetting, piezoelectric jetting, focused ultrasonic jetting, liquid spark jetting, etc. [11]. Thermal jets and piezo jets are the two most widely used DOD jetting techniques by commercial inkjet printers. Thermal jet, led by Canon and Hewlett-Packard, applies electrical pulses to heating elements in order to vaporize a small amount of liquid to produce bubbles in the fluid that create pressure pulses to eject droplets [12]. Piezoelectric jet, led by Epson, on the other hand, relies on the mechanical deformation of a piezoelectric element to produce the needed pressure pulse [13].

Although inkjet printing has great potential as a fabrication technique, it has been held back by a number of difficulties. One major difficulty is the printing speed is too slow. For instance, the build rate of injection molding (the "king" of mass production) is typically ~5000 cm^3/hour [14] while the build rate for inkjet is typically only ~100 cm^3/hour. To improve the printing speed, there are three different approaches, including increasing the number of nozzles, and/or the droplet size, and/or the printing frequency (i.e., the number of droplets generated per nozzle per second) [8].

Print heads with over 70,000 nozzles have been reported, but the nozzle number is limited by how many nozzles can be packed into a given area [15]. Droplet size is typically limited by the desired resolution. For example, for 600 DPI resolution, the droplet diameter needs to be smaller than ~50um. For printing frequency, most of commercial DOD inkjets print at ~10 kHz [8]. Although increasing printing frequency can lead to significant improvement of printing speed, little research has been reported on the limits of printing frequency and how it can be significantly increased. Despite hundreds of years of research on droplet formation dynamics, the understanding of droplet generation at high frequency remains elusive.

This paper presents a study on the printing frequency limit and the droplet generation dynamics at significantly higher frequency to improve printing speed for inkjet. First, previous research on the subject of droplet generation is reviewed and major issues involved in increasing the rate of droplet formation are identified. A numerical model is then developed, to simulate the droplet formation processes using a level-set interface tracking approach for the droplet-air interface. The simulation results are validated against experimental results from the literature [2]. Following this validation, the model is used to study the generation of droplets at MHz frequencies, with an objective of increasing the rate of material deposition. We find the key to produce droplets at high frequency is to increase the ejection velocity by increasing the energy input to the nozzle.

This paper is organized as follows. A literature review is presented in section 2. In section 3, a numerical model is developed to simulate the droplet formation dynamics. Experimental validation of the numerical model is provided in section 4. In section 5, the validated numerical model is then used to study droplet formation dynamics at megahertz frequency aided by the insights from scaling analysis. Conclusions are given in section 6.

2. LITERATURE REVIEW

This section provides an overview of what has been done in droplet ejection process of inkjet technology, including; reviews of the physics, waveform design, experimental investigations, and numerical models. J. Eggers (1997) performed a comprehensive review of the breakup in free-surface flows [16]. He found that the droplet formation mechanics can be approximated by one-dimensional equations at the point of breakup and still contain the majority of abundance of the original dynamics. In 2007 he worked in combination with E. Villermaux to provide a unified description of the physics behind droplet formation, including the effect of viscosity and the behavior of non-newtonian breakup [17]. A detailed review of the droplet dynamics by H. Wijshoff (2010), discussed different aspects of DOD specific processes, including pinch-off, the shape and size of droplets, formation of the droplet tail, and the formation and speed of satellite droplets [8]. Lin (1998) reported that the physical mechanisms involved in the breakup of liquid jets differed depending on the regimes of the relevant flow parameters. These are commonly referred to as the plateau, the first wind-induced, the second wind-induced, and the atomization regimes. Breakup in the plateau regime is dominated by surface tension. For the first wind-induced regime air resistance comes close to the magnitude of the surface tension, while for the second the air resistance surpasses the surface tension as the largest force [18]. Of course understanding how to balance these forces and what tools can be used to balance them, allows for control of this droplet formation behavior.

The driving waveform is one very important tool for controlling this droplet breakup. K. Kwon (2007) designed a two-pulse waveform for high-speed jetting based on the measured pressures in the print head to suppress the residual pressure waves after jetting [19] [20]. Iterative learning control (ILC) is a similar method employed by G. Wassinik et al., to design the input waveforms that ensure that droplet formation is unaffected by residual vibrations. Implementing the ILC controller design in the experimental setup allowed the error to be reduced by a factor of 5 [21].

An experimental technique for observing the droplet formation process was developed by H. Dong, W. Carr, & J. Morris (2006) using a pulsed laser, a low-speed charge coupled device camera, and a signal generator to record the droplet breakups. This process allows for a temporal resolution of 200 ns and a spatial resolution of 0.81 μm/pixel [22]. This technique was used to analyze experimental results and associate the observed breakup behaviors with changes to the input parameters of the system. It was found that a well-designed waveform allowed for the abrupt pinch-off of droplets, and the observation of two modes of breakup for the contracting liquid thread after pinch-off, end-pinching and multiple droplet breakup [2]. End pinching occurs when the tail of the liquid thread pinches off from the spherical droplet head, while the multiple droplet breakup was due to the presence of capillary waves [10]. J. Meacham et al. (2005) used ultrasonic driving frequencies ranging from ~1 MHz to ~5 MHz to induce breakup of water droplets from 1-10 μm nozzles from a micromachined droplet generator [23].

Research on numerical simulation has also been reported. Eggers one dimensional model for the behavior for droplet breakup showed surprisingly great results when used to simulate the behavior further away from the point of breakup; however, it is not capable of solving for both the microscopic and macroscopic phenomena at the same time [24]. G. Percin & B. Khuri-Yakub (2002) used a boundary integral to optimize a technique for droplet deposition [3]. D. Shin et al. compared the strengths and weaknesses of the one dimensional approach [25]. Meacham's research used Fluent to solve for droplet formation at driving frequencies in the MHz range. His research showed that frequency can be related to droplet size. From the literature survey it is clear that there is a gap in the research in producing droplets at higher frequencies up to the MHz range [24]. This paper covers that gap.

3. NUMERICAL MODELING

Due to the complex nature of droplet generation, some assumptions are made to simplify the analysis.

1) Since the fluid velocity involved is relatively small and the Mach number is well below 0.3, the fluid is considered incompressible.
2) Fluids are assumed to be Newtonian.
3) The liquid and the gas flow are both treated as laminar based on the low magnitude of the Reynolds number.

With the above assumptions, the form of the Navier-Stokes equations are as follows:

$$\rho \frac{\partial \boldsymbol{u}}{\partial t} + \rho(\boldsymbol{u} \cdot \nabla \boldsymbol{u}) = \nabla[-p\boldsymbol{I} + \boldsymbol{\eta}(\nabla \boldsymbol{u} + \nabla \boldsymbol{u}^T)] + \boldsymbol{F} \quad (1)$$

$$\nabla \cdot \boldsymbol{u} = 0 \quad (2)$$

where: ρ is the fluid's density in (kg/m^3); $\boldsymbol{u}$ is the velocity vector (m/s); p is the pressure (Pa); η is the dynamic viscosity (N·s/m^2); $\boldsymbol{F}$ is the body force; and $\boldsymbol{I}$ is the identity matrix [26].

In order to track the interface between the liquid and the air, the level-set approach is selected among many direct interface tracking approaches.

3.1. Level-Set Method

The physics of the droplet generation process falls into the category of multi-phase flow in fluid dynamics. Both the physical modeling and the numerical computation of this process present quite a challenge because of the moving interface between the two phases. There are many methods that can directly track phase interface, such as the phase-field method, the level-set method [26], the volume-of-fluid method, the boundary element method (BEM) with an adaptive mesh [8], and the front tracking method [27]. The level-set method was chosen for its simple formulation and accuracy. The level-set method provide direct tracking of the interface by simple convection of the interface with the flow field.

For the level-set approach, the interface is represented in space by the dimensionless number ϕ [27]. ϕ varies from 0 to 1. During the phase initialization step of the level-set approach the distance to the initial interface, D_{wi} is calculated so that the solver can use ϕ to differentiate between the two different fluids in the system. These two fluids are sorted so that for fluid 1 [26]:

$$\phi_0 = \frac{1}{1+e^{D_{wi}/\epsilon}} \quad (3)$$

and for fluid 2:

$$\phi_0 = \frac{1}{1+e^{-D_{wi}/\epsilon}} \quad (4)$$

In this way the domains in which fluid 1 is present and the domains in which fluid 2 is present will be properly filled with their respective fluids. This allows for the interface tracking equation to solve for the volume fraction of the fluids to differentiate the two fluid and simulate the movement of the ejected fluid. Regions of purely fluid 1 have a ϕ=0 and for those of fluid 2 ϕ=1, but for the areas where the regions meet, ϕ is between 0 and 1. The location of the interface is determined by the contour of ϕ=0.5. This interface is solved for using the following equations [28]:

$$\frac{\partial \phi}{\partial t} + \boldsymbol{u} \cdot \nabla \phi = \gamma \nabla \cdot (\varepsilon \nabla \phi - \phi(1-\phi)\frac{\nabla \phi}{|\nabla \phi|}) \quad (5)$$

where γ is the reinitialization parameter (m/s) that is typically set as the maximum speed of the flow and ε is the interface thickness controlling parameter (m) [26]. The density and dynamic viscosity then becomes a function of the level-set function:

$$\rho = \rho_1 + (\rho_2 - \rho_1)\phi \quad (6)$$

$$\eta = \eta_1 + (\eta_1 - \eta_1)\phi \quad (7)$$

where ρ_1 and ρ_2 are the densities and η_1 and η_2 are the dynamic viscosities of air and liquid respectively.

The combined body force vector **F** from equation (1) is broken down into its two parts: gravity represented by $\mathbf{F}_g$ and surface tension represented by $\mathbf{F}_{st}$. The definitions of the two parts of body force **F** are listed below:

$$\boldsymbol{F}_g = \rho \boldsymbol{g} \tag{8}$$

$$\boldsymbol{F}_{st} = \nabla \cdot (\sigma\left(\boldsymbol{I} - \left(\boldsymbol{n}\boldsymbol{n}^T\right)\right)\delta) \tag{9}$$

where: **g** is the gravity vector; σ is the surface tension (N/m); **n** is the vector normal to the interface; and δ is a smoothing approximation of the Dirac delta function (1/m) defined as:

$$\delta = 6|\nabla\phi||\phi(\mathbf{1} - \phi)| \tag{10}$$

3.2 Numerical Model

The numerical model was implemented with the commercially available software COMSOL 5.1. Given the symmetry of the geometry, the droplet system can be modeled axi-symmetrically as a nozzle ejecting into an air channel ending in a wetted substrate boundary. Figure 1 below, shows the configuration of the developed numerical model, and Table 1 gives the properties of the fluid 1 (air) and fluid 2 (distilled water) used in the simulation model.

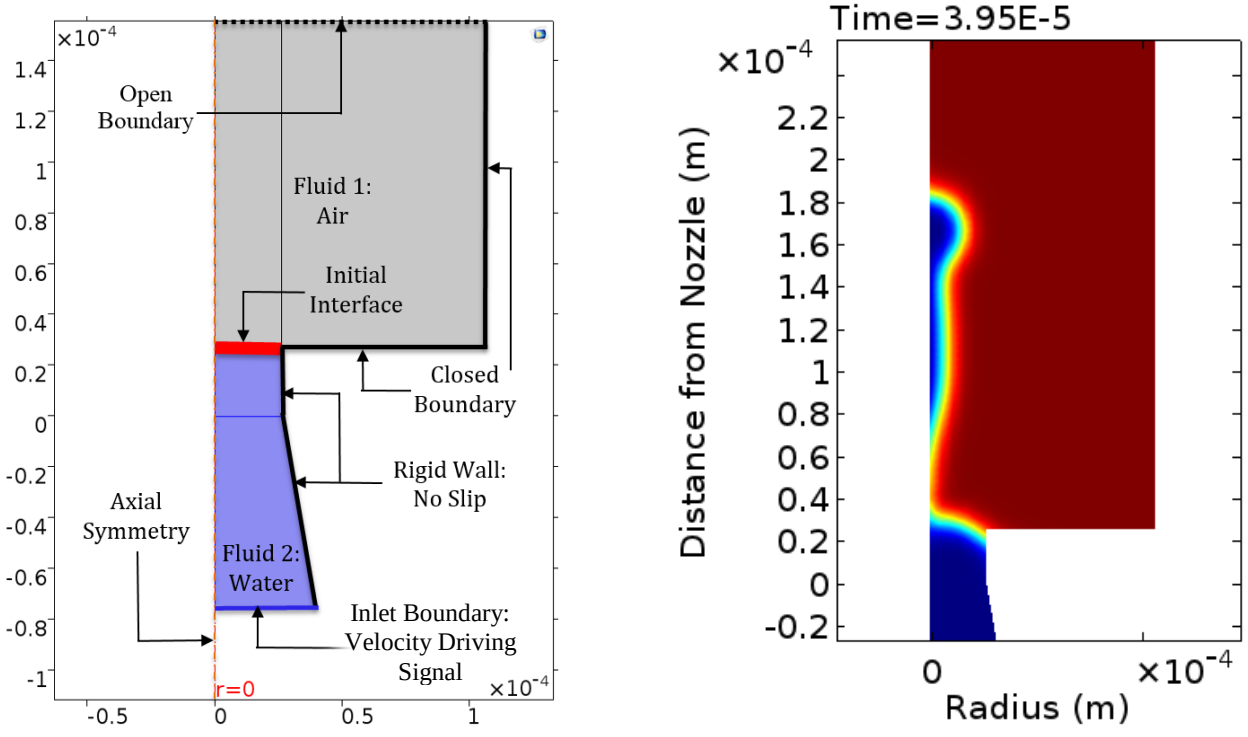

a) b)

Figure 1. a) Initial geometry of the model used in validation. The nozzle orifice and the initial interface are located at 26.5μm along the z-axis. The diameters of the nozzle inlet and outlet are 79.5μm and 53μm respectively. The boundary conditions are defined with descriptive callouts. Due to the negligible effects of gravity at this scale, the nozzle geometry is shown pointing directly up. b) Droplet ejection just after pinch-off.

The production of droplets is controlled by a velocity driving signal applied to the inlet boundary. The ejection of a droplet just after pinch-off is show in Figure 1 b), and the velocity of the droplet at the nozzle exit was 5.5m/s. The droplet is shown ejecting upwards for convenience as the effects of gravity are negligible at this length scale. Table 1 gives the properties of the fluid 1 (air) and fluid 2 (distilled water) used in the simulation model.

Table 1. Properties of Materials

Fluid #	Material	Density (kg/m^3)	Dynamic Viscosity (N·s/m^2)	Surface Tension (N/m)
Fluid 1	Air	1.225	1.789E-5	NA
Fluid 2	Distilled Water	1000	0.001	0.073

4. EXPERIMENTAL VALIDATION

Experimental results from Dong and Carr's [2] were used in critical comparison to the simulated results in order to validate the numerical model. The experiment used a 53µm diameter 75µm length nozzle pulsed by a bump mode piezo transducer to produce droplet breakup at a driving frequency of 20Hz [2]. The experimental results were recorded by measuring the position of the heads and tails of the main droplet and satellite droplets using the notation shown in Figure 2.

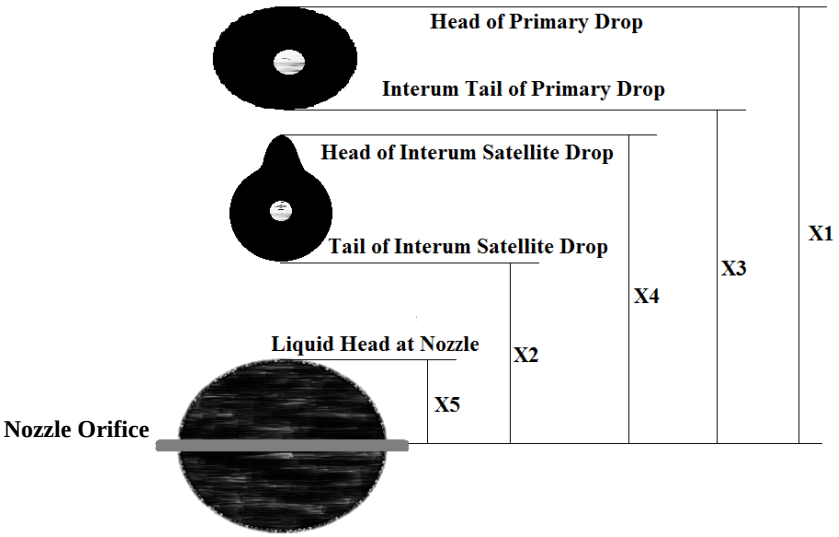

Figure 2. Nomenclature of the droplet breakup points as used in the experimental results [10]. The droplets are shown ejecting upwards. X1-X5 represent distances of different points on the droplet surfaces from the nozzle outlet. The points that X1-X5 reference are descriptively called out above.

To model the bump mode piezoelectric actuation of the distilled water, an inlet was modeled at the same depth (75µm) and approximate diameter (79.5µm) as in the nozzle. Because the displacement of the piezoelectric element is proportional to the voltage and velocity is the time derivative of displacement, an equivalent velocity driving signal is calculated to emulate the voltage driving signal in the literature, by taking the derivative of the voltage driving signal. The properties of the air and distilled water were used to define the respective fluids in COMSOL. The calculated velocity driving signal is show in Figure 3 below.

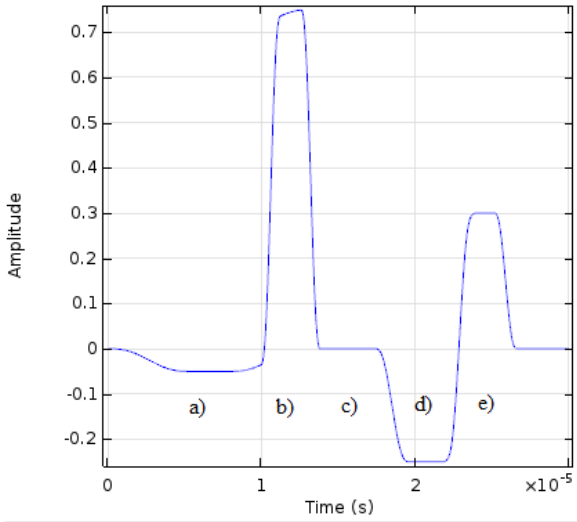

Figure 3. Driving signal for the inlet velocity of the simulation. a) The early negative pulse helps reduce residual vibrations. b) A fast positive pulse that forces the fluid out of the nozzle. c) Dwell time to let the inertia of the ejected fluid stretch and thin the liquid column as no more fluid is ejected out. d) The negative pulse causes suction back into the nozzle and simulates the contraction of the piezoelectric as it recharges on the second peak of the double-peak waveform. e) The small positive pulse simulates the discharge or the piezo-element at the end of the second peak and it acts to help refill the nozzle.

In combination with the driving signal shown above, an inlet velocity magnitude of ~10.9m/s was selected to match the exit velocity with the experiments this helped achieve the droplet formation shown by the experimental results.

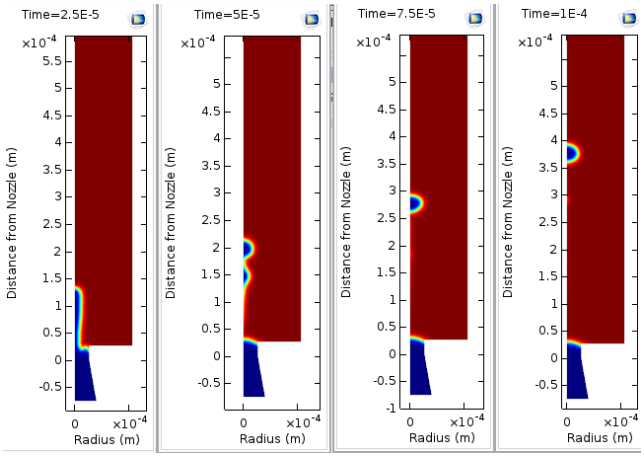

Figure 4. Two-dimensional illustration of the droplet formation in the simulation of the experimental conditions.

The simulation of the experimental results shown in Figure 4 show that shortly after droplet ejection, the tail of the primary drop breaks up to form a short lived satellite droplet. This droplet quickly recombined with the primary droplet as the size and undulations of the primary droplet stabilized for its flight path. This is consistent with what the experiment showed for the same droplet ejection conditions. The overall results of the simulation fit tightly with those found in the experiment. The results of the experiment detailing the distance of head and tail points for primary and satellite droplets from the nozzle over time were selected to compare with those of the simulation, as shown in Figure 5. Overall, the simulation results agree very well with the experimental data for the sophisticated droplet generation dynamics.

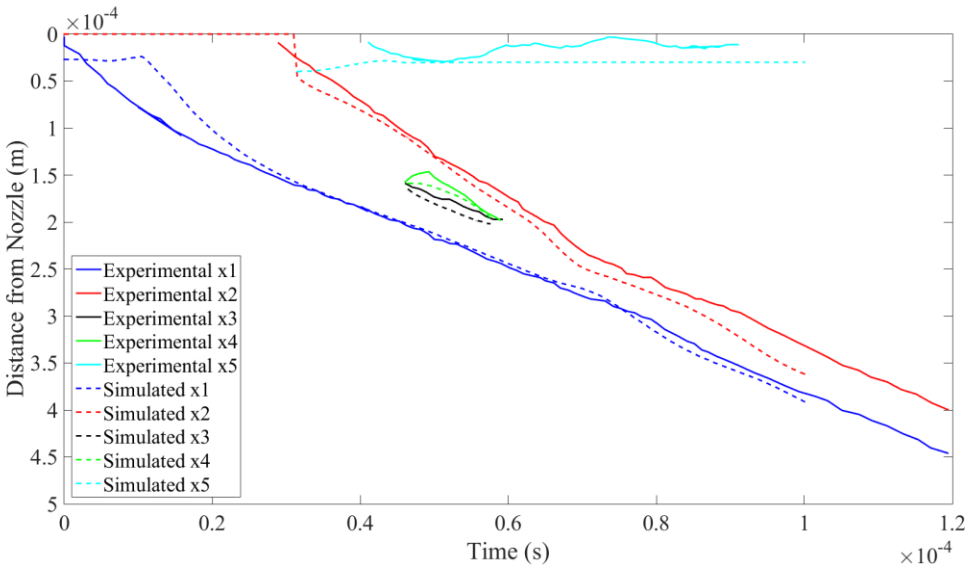

Figure 5. Comparison between experimental data and simulation

5. MHz FREQUENCY DROPLET GENERATION

The potential SFF applications of faster inkjet printing make MHz DOD drop formation of particular interest. Faster deposition rates will reduce the cost of additive manufacturing. This section tests our hypothesis that a high ejection velocity is the key to achieve high frequency droplet generation. Droplet generation was first observed at low frequencies for a given driving signal. The same system was then tested for the same ejection velocity at a higher frequency of driving signal and droplet generation did not occur. When the ejection velocity was increased to certain extent, droplet generation started to occur at the frequency of the driving signal. Scaling analysis was used to help estimate the required ejection velocity at the new frequency.

5.1. Scaling Analysis

For the process of drop formation, even small changes in nozzle geometry, driving frequency, input velocity, or fluid properties can have a great effect on the outcome. Because of this, there is a great difficulty in identifying proper system parameters for a desired behavior. Scaling analysis can provide approximate predictions of system behavior for different system parameters.

There are three primary forces that control the droplet formation dynamics: inertia, surface tension, and viscous force. Each force acts on certain length and time scales. Knowing the length and time scales of these forces would help identify the driving and resisting forces of the phenomena observed at a given time and length scale during the droplet formation process. With the scaling analysis, we would be able to estimate the outcome of the droplet formation dynamics from the input parameters [29].

Various timescales were used in comparison to help estimate what forces would dominate the system for increasing frequencies and velocities. The relevant timescales used in this present work are:

$$t_f = \frac{1}{f} \qquad (11)$$

$$t_U = \frac{D_0}{U} \quad (12)$$

$$t_\sigma = \sqrt{\frac{\rho {D_0}^3}{\sigma}} \quad (13)$$

where: t_f is the frequency timescale and f is the frequency of the driving signal; t_U is the inertial timescale and U is the magnitude of the ejection velocity; and t_σ is the surface tension timescale with D_o is the characteristic length approximately defined as the nozzle diameter.

In a typical inkjet printing cycle, surface tension is what drives the breakup of droplets. In order to achieve high frequency droplet generation, we need to match the droplet breakup frequency with the driving signal such that droplet breakup can occur within one cycle of the driving signal. Therefore the surface tension needs to act faster than the driving signal cycle and thus the value of t_σ needs to be less than the value of t_f. For this to be true for a given liquid (e.g., water), we have $D_0 < \left(t_f/\sqrt{\rho/\sigma}\right)^{2/3}$, which relates the diameter of the nozzle orifice to the frequency of the desired drop formation for water as seen in Figure 6. From this relationship, it becomes apparent that this regime of drop formation for current inkjet printers has a theoretical upper limit dictated by the relationship between droplet breakup frequency and nozzle diameter if surface tension is the primary driving force for the breakup.

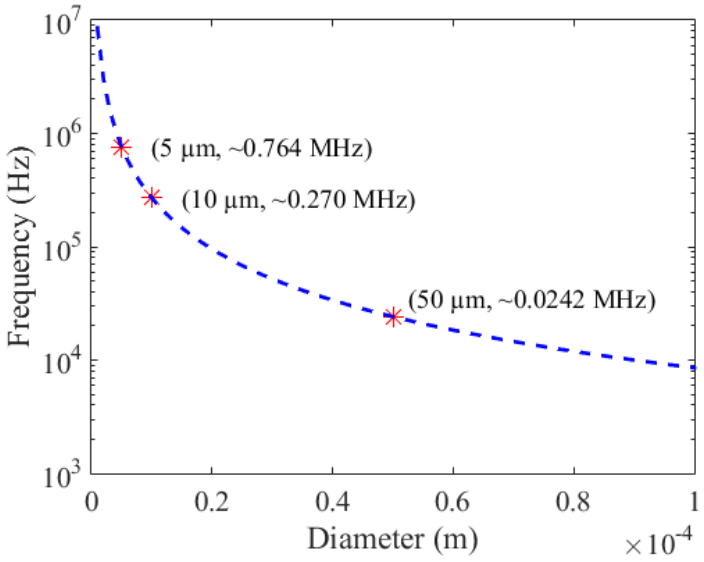

Figure 6. The relationship between the maximum plausible droplet formation frequency and different nozzle diameter based on scaling analysis. With points at 5µm, 10µm, and 50µm nozzle diameters.

Therefore, if the desired droplet generation frequency is greater than the upper frequency limit for a given nozzle diameter defined by the relationship in Figure 6, other sources of energy, such as kinetic energy, must provide support to drive the droplet breakup in the chosen time frame.

To continue analyzing the conditions under which droplet breakup occurs, it is necessary to identify three essential forces that exist in both the liquid and the air, involved in the development of droplets. These force scales are used to help find what force is acting as the primary driving force. The relevant controlling forces can be estimated as the following [27]:

$$F_p = \rho U^2 D_0^2 \quad (14)$$

$$F_\sigma = \sigma D_0 \quad (15)$$

$$F_{vis} = \eta U D_0 \quad (16)$$

where: F_p are the inertial forces, F_σ are the surface tension (capillary) forces, F_{vis} are the viscous forces. When the density of air is used for calculation, F_p becomes the inertial force of the air exerted on the liquid (i.e., the aerodynamic force or the air resistance). These three simplified forces were used to investigate the balance of forces in the transition from the first to second wind-induced regimes; however, differing approximations and more complex analyses do exist depending on the application and areas of specific interest *[17] [16] [30] [8] [29] [31] [32]*. Figure 7 below, shows the point where the inertial force from the air overcomes the surface tension force of the distilled water.

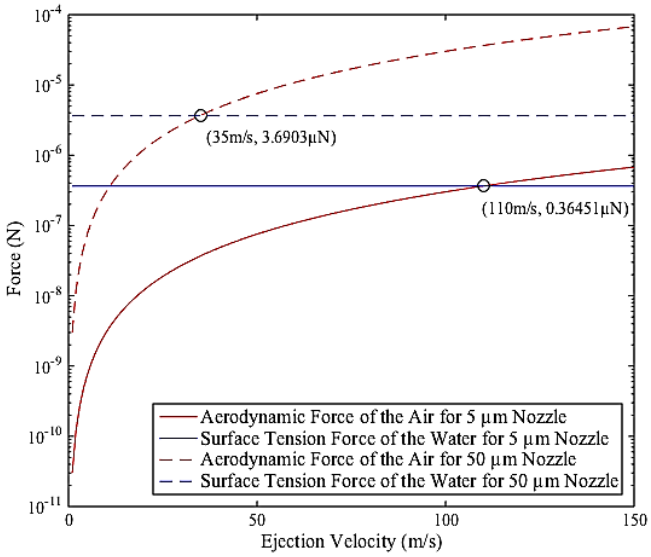

Figure 7. Illustration of two of the driving forces for droplet breakup, inertial force of the air (i.e., the aerodynamic force or the air resistance) in red and surface tension force of the water in blue vs. ejection velocity for the 5μm nozzle and) the 50μm nozzle respectively.

Given that for SFF manufacturing, our goal is to increase the deposition rate by speeding up current DOD drop formation into the MHz range from current ~10 kHz range for the production of similar sized droplets at much faster rates, the force analysis of interest becomes the balance of the inertial force of the air with the surface tension forces.

5.2. 5μm Nozzle

A small nozzle size was used on the first set of simulations, and the actual nozzle diameter was chosen to be 5μm. Prior consideration of the length and time scales showed that there is a theoretical soft upper limit for the frequency of droplet generation at any given nozzle size. For nozzles of 5μm in diameter the analysis of the system's length and time scales shows that breakup solely due capillary pinching is still likely for droplet generation at frequencies up to ~764 kHz, as evident in Table 2 below:

Table 2. Calculations for the values of the frequency and surface tension timescales with their difference used to estimate the frequency at which the droplet ejection will have to rely on other forces in addition to surface tension to obtain breakup.

Diameter (m)	ρ (kg/m^3)	η (N*s/m^2)	σ (N/m)
5.00E-06	1000	1.00E-03	0.073

Frequency (MHz)	t_f (µs)	t_σ (µs)	t_f-t_σ (µs)
0.1	10	1.31	>0
0.764	1.31	1.31	=0
1	1	1.31	<0
2.5	0.4	1.31	<0

While this is an estimate of the upper limit for capillary pinching, we believed we could still produce droplets uniformly beyond this limit with a greater magnitude of input energy. Therefore to develop a better understanding of the role input energy density plays in the formation of droplets at increasing frequencies, droplet generation from a 5µm nozzle is studied for velocity driving signal frequencies of 100 kHz, 1 MHz, and 2.5 MHz.

The dimensions of the 5µm diameter nozzle geometry are 10µm in diameter at the inlet and 5µm at the outlet, 25µm in nozzle inlet length, with a 0.1mm channel length (refer to Fig. 1). To help analyze the simulation and obtain graphical data of the droplet generation, the leading and lagging points of every droplet were plotted with the following notation shown in Figure 8 below.

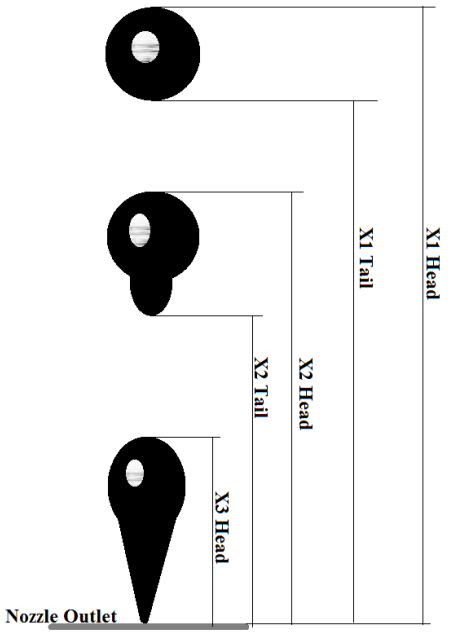

Figure 8. An illustration of the notation style used to describe points of droplet breakup. The droplets are shown traveling upward. The nozzle would be below the frame of reference shown in the illustration above.

5.2.1. 100 kHz

For the 5µm diameter of the nozzle, 100 kHz is at relatively low frequency because the timescale of the surface tension is well within one cycle of the driving signal. The breakup behavior of the

5μm nozzle diameter droplet model at 100 kHz was found at ~20m/s ejection velocity. Figure 9 shows the distance from the nozzle vs time for the first 5 droplets formed. Each colored marker represents the head and tail of a droplet. From the nearly parallel change of the positions of the head and tail for each droplet, we can tell the deformation and oscillation of the droplets are negligible. As we can also see from the nearly equal interval between different markers, the droplets are produced at a nearly constant rate and uniformly distributed, which is a desirable outcome for inkjet printing. The droplets show deceleration over time mostly due to the resistive force of the air drag.

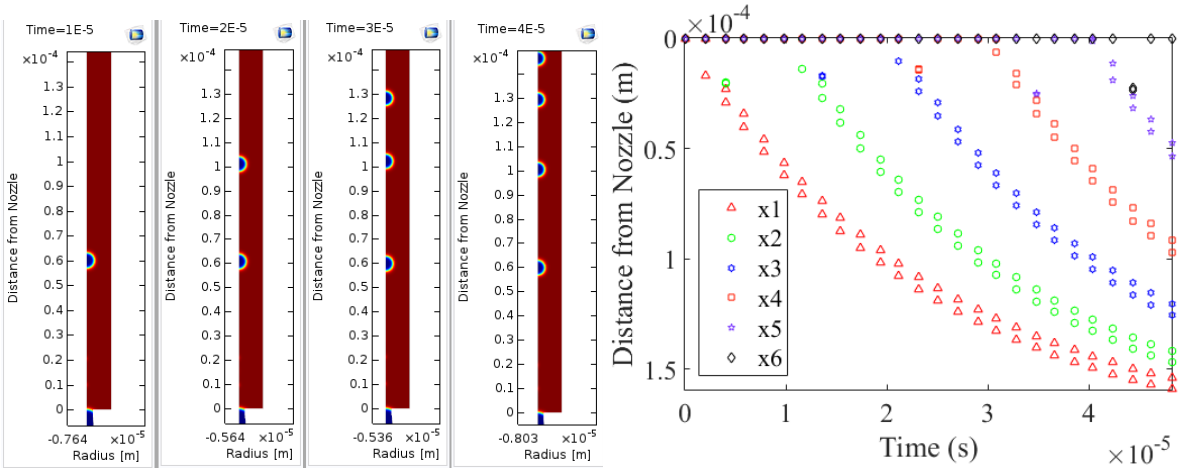

Figure 9. a) Two dimensional illustrations of droplets travelling along the air channel at four equally spaced distinct instants in time during the droplet generation. b) Distance from nozzle of droplet heads (leading pictorial marker) and tails (lagging pictorial marker) as a function of time.

5.2.2. 1 MHz

The analysis of the timescales shown in Table 2 predicts that for a frequency of 1 MHz more than just the efforts of the surface tension forces will be required for droplet generation at a rate of one droplet per driving signal cycle. The results of running the simulation at a higher frequency with an ejection velocity of ~20 m/s as shown before are shown below in Figure 10.

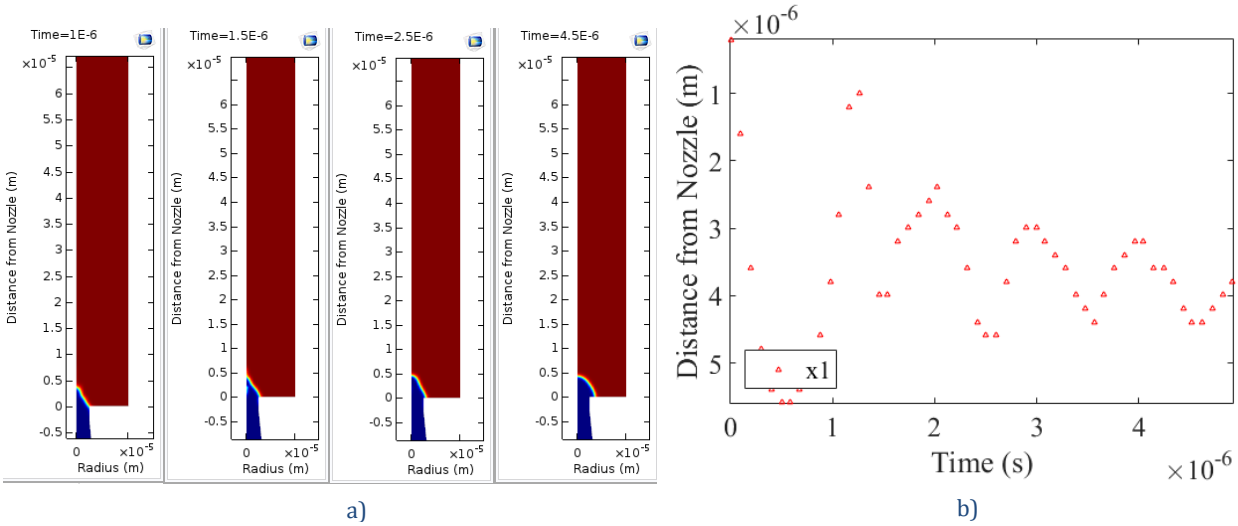

Figure 10. Shows the results of running the simulation at 1MHz with the same magnitude of the ejection velocity as used at 100 kHz. a) A two dimensional illustration of the fluctuations in the liquid column. Notice that no attempt at droplet ejection is observed instead the low energy is only capable of pushing out small amounts of liquid and making outer surface fluctuate. b) The study of the distance from the nozzle vs. time shows that the increase in liquid volume outside the nozzle with every velocity pulse mimics a harmonic decay in the fluctuation of the mass.

Figure 10 shows that the subsequent fluid ejections did not result in droplet formation but rather that the growing mass of fluid had an increasing damping effect on the energy ejected. The simulation results for the 1 MHz driving frequency are shown below in Figure 11 and seem to corroborate hypothesis for the need to increase the magnitude of the ejection velocity.

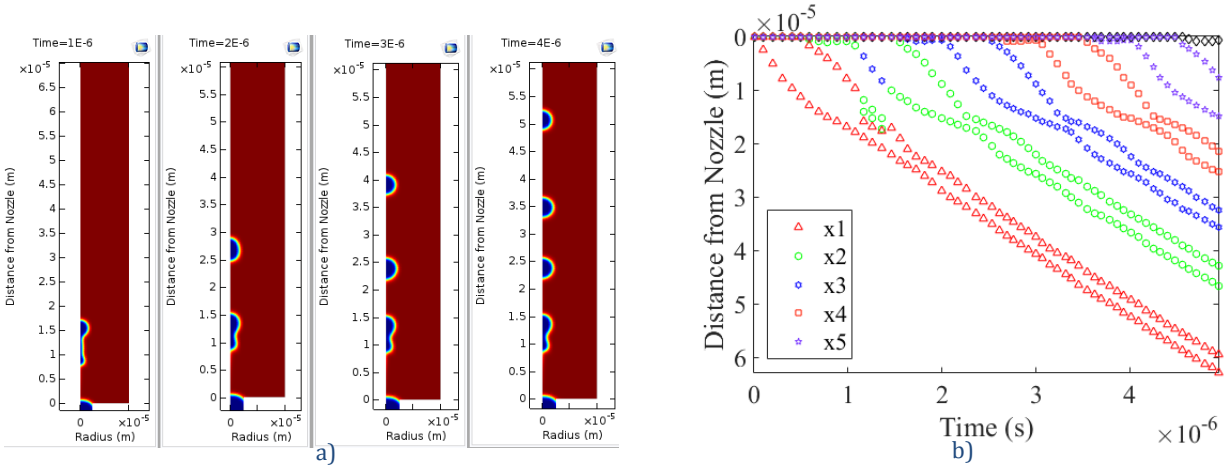

Figure 11. Shows the ejection of droplets and their flight through the air channel. a) A two dimensional illustration of the droplets traveling down the air channel at four distinct instances in time. Notice that the liquid tail is still shown recoiling into the primary droplet even at a slightly greater distance from the nozzle. This is primarily due to the greater speed at which the droplets are traveling and the drag of the aerodynamic forces on the droplet at this greater speed. b) Distance from the nozzle of the droplet heads and tails as a function of time for a 5μm nozzle diameter driven at 1 MHz.

For the droplet generation at 1 MHz shown in Figure 11 b) the ejection velocity was found to be ~30m/s. At this ejection velocity the magnitude of the air resistance is 27.1 nN while the surface tension is at 364 nN. Since the air resistance is close to 10% of the surface tension force, it start to play an assistive role to shorten the time scale of the droplet breakup (i.e., beyond the timescale of the surface tension). In comparison with the 100 kHz case, which has an abrupt thinning; the thinning at this frequency was much more gradual, which suggests that the air resistance is playing a role in the thinning process. Unlike previous simulations, the droplets show clear signs of deformation after breaking from the liquid column as shown in Figure 11 b), as indicated by the difference between the droplet head and the droplet tail. This is primarily due to the large influence of the air's inertial force at this level. The inertia of the air, as a reactionary force, is increase by the inertia of the ejecting liquid. Figure 11 a) contains illustrative snapshots of the droplet breakup behavior shown above. Each frame shows the recoil of the liquid tail into the primary droplet causing the droplet to deform and oscillate back to its spherical equilibrium.

5.2.3. 2.5 MHz

The simulation of the droplet generation for 2.5 MHz at the same ejection velocity as at 1 MHz, produced ripples in the growing liquid column, but failed to produce droplets. In order to produce one droplet per cycle of the driving signal, we increased the ejection velocity to ~50m/s. The results the droplet generation process are shown in Figure 12.

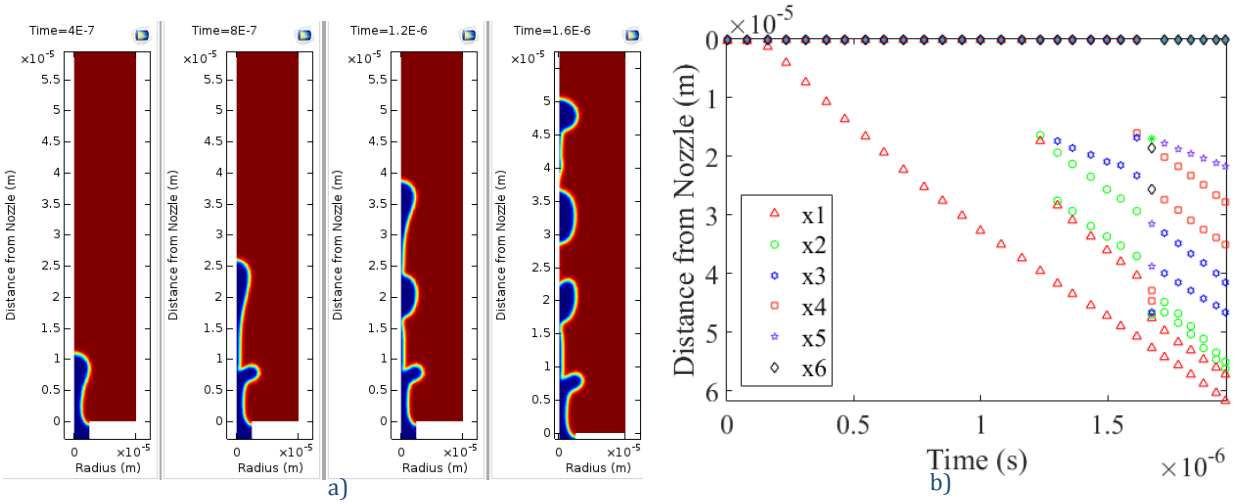

Figure 12. a) A two dimensional illustration of the droplet generation driven at 2.5 MHZ with sufficient input energy to cause droplet formation. b) Distance from the nozzle of the droplet heads and tails as a function of time for a 5μm nozzle diameter driven at 2.5 MHz. In this system the droplets did not pinch-off at the nozzle exit but were carried out away from the nozzle by the next ejection of fluid.

Unlike the 1 MHz case shown in Figure 11, the separation of the droplets occurs further away from the nozzle as shown in Figure 12 a), possibly because the surface tension breakup is slower than the cycle of the driving signal. This causes a delay (i.e. the droplets are not fully generated within their driving cycle) in the breakup of the droplets; however, the droplets are still generated at the same frequency as the driving signal. As can be seen from Figure 12, the droplets can still be produced uniformly. The magnitude of the air resistance is at 75.3 nN but is still less than the forces of the surface tension at 364 nN. With the aerodynamic forces at ~20% of the surface tension forces, it is clear that both will play a major role in the droplet breakup behavior.

5.3. 50μm Nozzle

In order to increase the printing speed of inkjet, the material deposition rate (i.e., volume of materials deposited per unit time) needs to be improved. Droplet volume is critical to this mission; therefore, printing larger droplets at a high frequency is of particular interest to us. Because of this, we will investigate the droplet breakup behavior for droplet size of ~50μm. The upper cap for the frequency of the driving signal was found at ~24.2kHz, as evident in below:

Table 3. Calculations for the values of the frequency and surface tension timescales with their difference used to estimate the frequency at which the droplet ejection will have to rely on other forces in addition to surface tension to obtain breakup.

Diameter (m)	**ρ (kg/m^3)**	**η (N*s/m^2)**	**σ (N/m)**
5.00E-05	1000	1.00E-03	0.073

Frequency (kHz)	**t_f (μs)**	**t_σ (μs)**	**t_f-t_σ (μs)**
10	100	41.3	> 0
24.2	41.3	41.3	= 0

100	10	41.3	< 0
1000	1	41.3	< 0

Therefore to develop a better understanding of the role input energy density plays in the formation of droplets at increasing frequencies, droplet generation from a 50µm nozzle is studied for input values at 10 kHz and 100 kHz.

The dimensions of the nozzle in this section are 50µm diameter at the outlet and a 230µm nozzle diameter at the inlet with a distance of 200µm between the inlet and outlet. The air channel length was set at 2mm, and the choice of the dimensions used in this section were chosen to standardize the sizes that were based on the scaling analysis.

5.3.1. 10 kHz

The breakup behavior of the 50µm nozzle diameter droplet model at 10 kHz was found at ~5m/s ejection velocity, which is comparable to the typical ejection velocity of the commercial inkjet printers (typically ~5 to 10 m/s) for this droplet size. Figure 13 b), below shows the distance from the nozzle vs. time for the first 5 droplets formed. The visualization of the droplet breakup is shown in Figure 13 a).

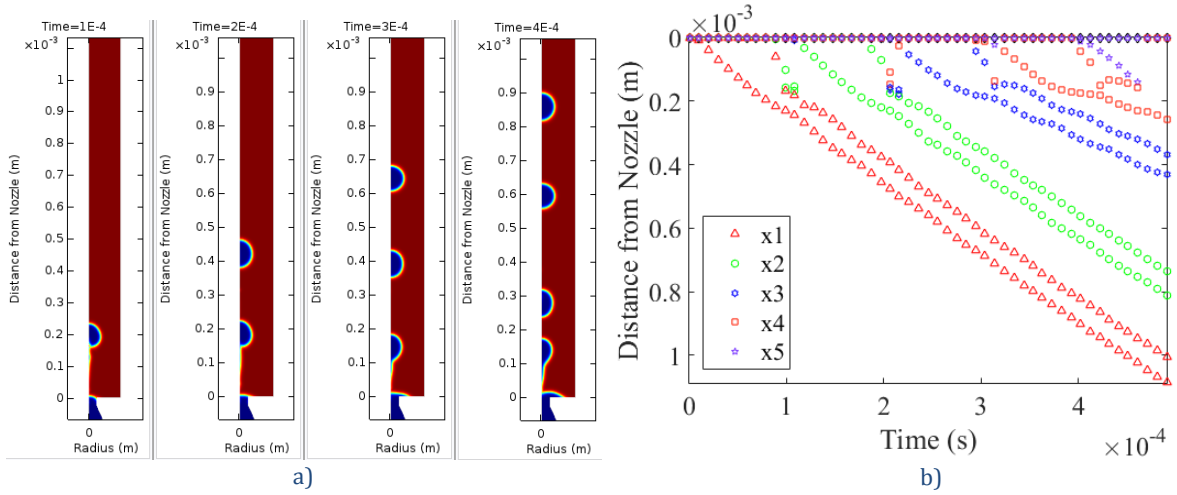

a) b)

Figure 13. a) Shows an illustration of the droplet breakup and flight in the air channel at a 10 kHz frequency for the velocity driving signal. b) A graphical representation of the distance from the nozzle of the droplet heads and tails as a function of time for a 50µm nozzle diameter driven at 10 kHz. Droplets are shown to exceed

The droplet generation shown above shows the formation of distinct droplets with only minor oscillations in the droplet shape after breakup form the liquid column. These oscillations are shown by the change in the length of the droplet from top to bottom right after breaking off from the fluid still connected to the nozzle. This growth is seen in the waves in the curves that plot the position of the droplet points from the nozzle. This stable behavior is also consistent given the similarity in the size of the droplets as shown above. The common behavior of temporary satellite droplet formation is observed early in the process, just after ejection. The satellites quickly recombine with their respective primary droplets. The clear presence of droplet deformation and oscillations, even though the droplets were ejected at a relatively low velocity, is due to the larger mass of the ~50µm diameter droplets compared to their ~5µm counterparts shown earlier. With this low ejection velocity the air resistance is only 75.3 nN making it about 2% of the surface tension forces

at 3.64 µN. Therefore air resistance does not play a major role in the breakup behave of the droplets at this frequency.

5.3.2. 100 kHz

When the model was run at 100 kHz with the same ejection velocity as the 10 kHz case, each pulse of the driving signal caused the liquid mass forming at the end of the nozzle to grow in volume, but continued to lack sufficient energy for droplets to be ejected. Instead each burst of fluid from the droplet just caused the liquid mass to wiggle and grow. For droplet generation solely due to the forces of surface tension, the scaling analysis predicted that the maximum frequency possible for 50µm nozzles was ~24.2 kHz (Table 3). Therefore, we chose to investigate droplet generation at 100 kHz to ensure that the effects of the air resistance would play a significant role in the droplet breakup. We found that an ejection velocity of ~15m/s was necessary for generating droplets at the same frequency as the driving signal. The measurements of the distance from the nozzle versus time are shown in Figure 14 b).

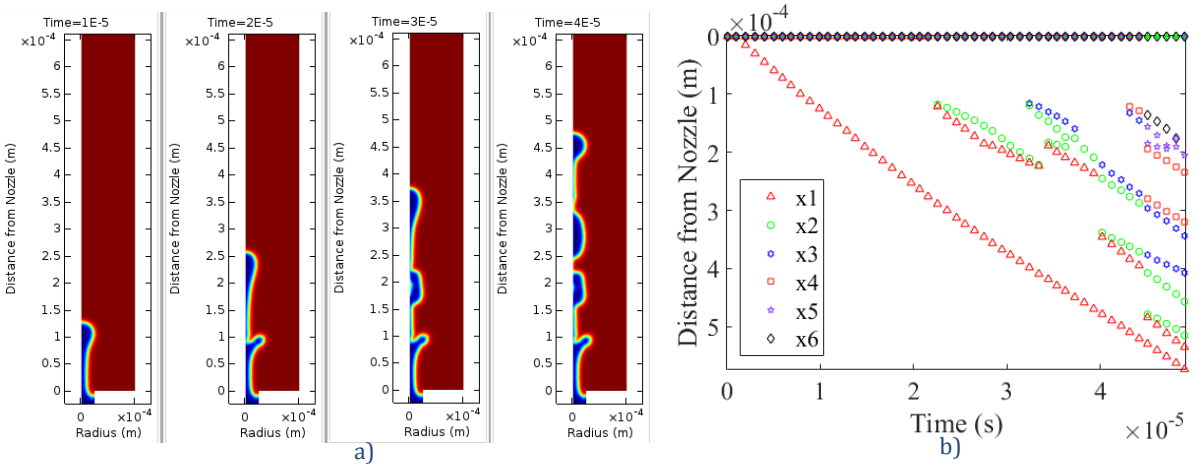

Figure 14. a) Two dimensional illustration of the droplet generation from a 50µm nozzle driven at 100k kHz with sufficient inlet energy to cause droplet ejection. Here we see how the aerodynamic forces of the air cause a concave shape in the following droplet, this phenomena helps to slow down the droplets following the first to allow the first sufficient distance and time to stretch, thin, and pinch-off. b) Distance from nozzle of the heads and tails of droplets as a function of time for the 50um nozzle diameter driven at 100 kHz.

Unlike the 10 kHz case shown in Figure 13, as approximately 20% of the surface tension forces, which are at 3.64 µN, while the magnitude of the air resistance is at 678 nN. So like the 2.5 MHz 5µm case shown in Figure 12 a), the air resistance plays a significant role in the droplet breakup at this frequency and length scale. Similarly, droplets are still generated at the same frequency as the driving signal, despite the delay caused by the surface tension breakup occurring slower than the cycle of the driving signal. This is possibly the reason for the separation of droplet further away from the nozzle than in the 10 kHz case shown in Figure 13 a). The droplets can still be produced uniformly as shown in Figure 14 a).

The unusual shape of all the droplet heads is most likely the result of the air resistance pushing them outwards and increasing their surface area. After the leading droplet pinches off form the liquid column, a cavity is formed by the extended arm of the following droplet swinging up and catching the escaping tail. One possible explanation for this behavior is that the surface tension was only capable of overcoming the air resistance pushing on the following droplet, after the load

of the leading droplet was relieved by its breakup from the liquid column. This phenomenon is shown in the third instance of time and by the appearance of a short lived cavity in Figure 14 a) and b) respectively.

6. CONCLUSIONS

This paper was set out to investigate possible approaches to boost the printing frequency of inkjet in order to significantly improve the printing speed of inkjet and make it a cost-efficient digital manufacturing method compared to traditional manufacturing. First, we reviewed the literature on droplet generation dynamics and found little research on the dynamics at high frequency. In order to study the droplet generation dynamics at high frequency, we developed a numerical model to simulate the droplet generation process using the level-set approach and validated the numerical model with experimental data obtained from literature. Aided by a scaling analysis, which showed the droplet breakup frequency was limited by the timescale of surface tension, simulations with the experimentally validated model were performed to test the hypothesis that increasing the ejection velocity would help increase the droplet breakup frequency to beyond the limit imposed by surface tension. It was found when ejection velocity is increased to a certain extent such that the air resistance is comparable to surface tension, the droplet generation frequency can be increased to beyond the current inkjet printing frequency from ~10 kHz to ~100 kHz or even ~1 MHz. The findings have important implication in significantly increasing the printing speed of inkjet and make it a cost-efficient digital manufacturing method.

7. Acknowledgements

We gratefully acknowledge the financial support from the University of Arkansas, through the startup fund provided by the Vice Provost Office for Research and Economic Development. Any opinions, findings, and conclusions or recommendations expressed in this publication are those of the authors and do not necessarily reflect the views of the University of Arkansas.

8. References

[1] D. Jang, D. Kim and J. Moon, "Influence of Fluid Physical Properties on Ink-Jet Printability," *Langmuir,* vol. 24, pp. 2629-2635, 2009.

[2] H. Dong and W. W. Carr, "An Experimental Study of Drop-on-Demand Drop Formation," *Physics of Fluids,* vol. 18, no. 7, pp. 1-16, 2006.

[3] G. Percin and B. T. Khuri-Yakub, "Piezoelectric Droplet Ejector for Ink-Jet Printing of Fluids and Solid Particles," *Review of Scientific Instruments,* vol. 74, no. 2, pp. 1120-1127, 2003.

[4] B.-J. de Gans and U. S. Schubert, "Inkjet Printing of Polymer Micro-Arrays and Libraries: Instrumentation, Requirements, and Perspectives," *Macromolecular Rapid Communications,* vol. 24, pp. 659-666, 2003.

[5] A. H. Rida, "Cunductive Inkjet Printed ANtennas on Flexible Low-Cost Paper-Based Substrates for RFID and WSN Applications," Georgia Institute of Technology, Atlanta, 2009.

[6] B.-J. de Gans, P. C. Duinveld and U. S. Schubert, "Inkjet Printing of Polymers: State of the Art and Future Developments," *Advanced Materials,* Vols. 203-213, no. 3, p. 16, 2004.

[7] M. Singh, H. M. Haverinen, P. Dhagat and G. E. Jabbour, "Inkjet Printing-Process and Its Applications," *Advanced Materials,* vol. 22, pp. 673-685, 2010.

[8] H. Wijshoff, "The Dynamics of the Piezo Electric Printhead Operation," *Physics Reports,* vol. 491, pp. 77-177, 2010.

[9] W. Van Hoeve, S. Gekle, J. H. Snoejer, M. Versluis, M. P. Brenner and D. Lohse, "Breakup of Diminuative Rayleigh Jets," *Physics of Fluids,* vol. 22, pp. 1-11, 2010.

[10] H. Dong, *Drop-on-Demand Inkjet Drop Formation and Depostioin,* Georgia Institute of Technology, 2006.

[11] H. P. Le, "Progress and Trends in Ink-jet Printing Technology," *Journal of Imaging Science and Technology,* vol. 42, pp. 49-62, 1998.

[12] N. J. Nielson, "History of Thinkjet Printhead Development," *Hewlet-Packard Journal,* vol. 36, no. 5, pp. 7-10, 1985.

[13] K. Uchino, "Piezoelectric Actuators 2006," International Center for Actuators and transducers Materials Research Institute , University Park, 2006.

[14] F. Johnannaber, Injection Molding Machines A User's Guide, Munich: Carl Hanser Verlag, 2008.

[15] Memjet, "One Printhead, Many Industries," Memjet, 2015. [Online]. Available: http://www.memjet.com/technology/printhead. [Accessed 8 August 2015].

[16] J. Eggers, "Nonlinear Dynamics and Breakup of Free-Surface Flows," *Reviews of Modern Physicsf,* vol. 69, no. 3, pp. 865-929, 1997.

[17] J. Eggers and E. Villermaux, "Physics of Liquid Jets," *Reports on Progress in Physics,* vol. 71, no. 036601, pp. 1-79, 2008.

[18] S. P. Lin and R. D. Reitz, "Drop and Spray Formation form a Liquid Jet," *Fluid Mechanics,* vol. 30, pp. 85-105, 1998.

[19] K.-S. Kwon and W. Kim, "A Waveform Design Method for High-Speed Inkjet Printing Based on Self-Sensing Measurment," *Sensors and Actuators,* vol. 140, no. A, pp. 75-83, 16 May 2007.

[20] K.-S. Kwon, "Experimental Analysis of Waveform Effects of Satellite and Ligament Behavior via in situ Measurment of the Drop-On-Demand Drop Formation Curve and the Instantaneos Jetting Speed Curve," *Journal of Micromechanics and Microengineering,* vol. 20, pp. 1-14, 2010.

[21] M. G. Wassink, N. Bosch, O. H. Bosgra and S. Koekebakker, "Enabling Higher Jet Frequencies," Oce-Technologies B. V. .

[22] H. Dong, W. W. Carr and J. Morris, "Visuliation of Drop-onDemand Inkjet: Drop Formation and Deposition," *Review of Scientific Instruments,* vol. 77, pp. 1-8, 2006.

[23] J. M. Meacham, M. Varady, F. L. Degertekin and A. G. Fedorov, "Droplet Formation and Ejection from a Micromachined Ultrasonic Droplet Generator: Visualization and Scaling," *Physics of Fluids,* vol. 17, pp. 1-8, 2005.

[24] J. M. Meacham, "A Micromachined Ultrasonic Droplet Generator: Design, Fabrication, Visualization, and Modeling," Georgia Institure of Technology, 2006.

[25] D.-Y. Shin, P. Grassia and B. Derby, "Numerical and Experimental Comparisons of Mass Transport Rate in a Piezoelectric Drop-on-Demand in et Print Head," *International Journal of Mechanical Sciences,* vol. 46, pp. 181-199, 2004.

[26] COMSOL Multiphysics, "Theory for the Level Set and Phase Field Interfaces," COMSOL Multiphysics.

[27] W. Zhou, "Interface Dynamics in Inkjet Deposition," Georgia Institute of Technology, Atlanta, 2014.

[28] H. Grzybowski and R. Mosdorf, "Modelling of Two-Phase Flow in a Minichannel using Level-Set Method," *Journal of Physics: Conference Series* , vol. 530, pp. 1-8, 2014.

[29] G. Christopher and S. L. Anna, "Topical Review: Microfluidic Methods for Generating Continuous Droplet Streams," *Journal of Physics D: Applied Physics,* vol. 40, pp. R319-R336, 2007.

[30] T. A. Kowalewski, "ON the Seperation of Droplets from a Liquid Jet," *Fluid Dynamics Research,* vol. 17, pp. 121-145, 1996.

[31] M. Mseler and U. Landman, "Formation. Stability, and Breakup of Nanojets," *Science,* vol. 289, pp. 1165-1169, 2000.

[32] J. Q. Feng, "A General Fluid Dynamic Analysis of Drop Ejection in Drop-on-Demand Ink Jet Devices," *Journal of Imaging Science and Technology,* vol. 46, no. 5, pp. 398-408, 2002.